

journal homepage: <http://civiljournal.semnan.ac.ir/>

Comparative Review of the Performance Based Design of Building Structures Using Static Non-Linear Analysis, Part B: R/C Frames

R. C. Barros¹, M.T. Braz-César², H. Naderpour^{3*} and S.M. Khatami⁴

1. Associate Professor, Faculty of Engineering, Civil Engng Dept, University of Porto (FEUP), Porto, Portugal.

2. Ph.D. Student, Faculty of Engineering, Civil Engng Dept, University of Porto (FEUP), Porto, Portugal.

3. Assistant Professor, Faculty of Civil Engineering, Semnan University, Semnan, Iran.

4. Ph.D. Student, Faculty of Civil Engineering, Semnan University, Semnan, Iran.

*Corresponding author: naderpour@semnan.ac.ir

ARTICLE INFO

Article history:

Received: 14 October 2013

Accepted: 24 November 2013

Keywords:

Performance based design,

Static non-linear analysis,

Pushover,

Bracing system,

Dynamic analysis.

ABSTRACT

The objective of this review to be submitted in two independent parts, for steel frames and for RC frames, is to compare their structural performance with respect to the proposed N2-method, and so also of the consequent convenience of using pushover methodology for the seismic analysis of these structures. A preliminary investigation is presented on a pushover analysis used for the seismic performance of metallic braced frames equipped with diagonal X-bracing and K-bracing systems. Three steel frames are analysed corresponding to 3, 6 and 10 floor regular buildings that were modelled in the MIDAS/Civil finite element software. To obtain the pushover curve a non-linear static methodology is used. For the RC frames three commercial programs (SAP 2000, SeismoStruck and MIDAS/Civil) are used in order to perform a parametric study based on pushover analyses. The equivalent strut method is applied to simulate the influence of the masonry infill panels; to evaluate the influence of these on the capacity curves, several strut width values are considered. The parametric study also addresses the influence of other parameters on the structural behaviour and non-linear capacity curves of the RC frame, namely: length and position of the plastic hinges and different loading patterns (uniform, modal and triangular distributions).

3. Comparative PUSHOVER ANALYSES OF R/C FRAMES

3.1. Introduction

The pushover analysis can be an easy and efficient technique to study the response of

R/C buildings under seismic actions. In this case, the sequence of component cracking, yielding and failure, as well as the deformation pattern and shear evolution in the structure, can be traced as the lateral loads or displacements are increased. The main difference between the steel and R/C analysis is obviously related with the material behaviour and therefore the plastic hinge properties. The R/C hinge model must consider the nonlinear behaviour of structure, quantified by strength and deformation capacities. The assessment of these plastic hinge constitutive laws is the central difficulty to use a nonlinear procedure. However, when accurate plastic hinge behaviour is obtained then an analogous to the previous pushover procedure can be performed to evaluate the response of the structural system.

This section addresses some of the relevant issues regarding the use of a nonlinear static procedure to study the response of R/C buildings. Finally, to exemplify the relevance of this analysis several simplified R/C frames were studied.

3.2. R/C Plastic Hinges

Lumped plasticity is a common approach to estimate the deformation capacity of R/C

elements. The ultimate deformation capacity of an element depends on the curvature and plastic hinge length and the use of different criteria for these parameters may result in different deformation capacities. In the past years, several plastic hinge lengths have been proposed and also several plastic hinge nature. Some authors have proposed a number of expressions in order to establish the correct hinge length (Table 2).

The plastic hinges are usually located near to the elements ends where the cracking process begins due to bending moment. However, to correctly simulate the hinge behaviour it is necessary to consider the structural function of each element. To characterize the hinges located in the columns it is necessary to compute the axial force and bending moments interaction (P-My-Mz), therefore is fundamental to obtain the interaction curves. By other hand, beams can be simulated only with the bending moments (My-Mz) contribution and finally, the masonry walls can be simulated considering only the axial force (P) because masonry panels are accurately simulated with equivalent ties with compression behaviour only.

Table 2. Plastic hinge length.

Reference	Hinge Length
Park and Paulay [22]	$L_p = 0,5 \cdot h$
Park, Priestley and Gill [23]	$L_p = 0,08 \cdot L + 6 \cdot d_b$
Priestley, Seible and Calvi [24]	$L_p = 0,08 \cdot L_c + 0,022 \cdot f_{ye} \cdot d_b \geq 0,044 \cdot f_{ye} \cdot d_b$

L_p - plastic hinge length h - cross section height f_{ye} - yield strength of the longitudinal bars
 L_c - distance between the plastic hinge and the null bending moment d_b - reinforcement steel bar diameter

3.3. Masonry Infill Panels

Masonry panels are normally neglected during the design procedure; however the use of their resistance capacity in this process can considerably improve the structural seismic behaviour. Furthermore, the failure mode of a masonry filled frame is normally difficult to predict since the collapse of the frame-masonry system can occur in the masonry infill as well as in the frame depending on several factors as the frame and infill panel stiffness ratio, the strength of their components and the dimensions of the structure.

Figure 14 illustrates the some of the most significant masonry failure mechanisms: debonding of the mortar joints, cracking or crushing of the masonry units (or a combination of these modes). The importance of each failure mechanism depends on the material properties and the stress state induced in the panel and the filled frame collapse usually results from a combination of these mechanisms. However, the local failure of one component does not

represent the failure of the whole system and should be regarded only as a serviceability state.

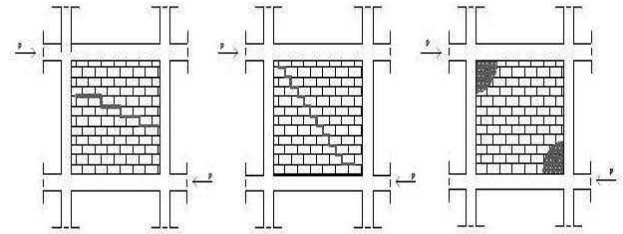


Fig. 14. Modes of failure of masonry walls

Among the frequent failure modes (Table 3) the shear cracking in masonry panels due to shear stresses is the most common failure mode observed in the experimental research. This mode is mainly controlled by the shear strength of the mortar joints (bond strength and coefficient of friction), the tensile strength of the masonry units and the shear and normal stresses ratios.

Depending on these parameters, the combination of shear stresses with vertical axial stresses can produce either cracks crossing the masonry units or debonding along the mortar joints (also termed as shear friction failure).

Table 3. Masonry panels failure modes.

Shear Cracking	<ul style="list-style-type: none"> i) Stepped Cracking Along the Mortar Joints; ii) Horizontal Sliding Along the Mortar Joints; iii) Cracking Due to Diagonal Tension.
Compressive failure	<ul style="list-style-type: none"> i) Crushing of the Loaded Corners; ii) Compressive Failure of the Diagonal Strut.
Flexural cracking	Flexural cracks can open in the tensile side of the panel due to the low tensile strength of the masonry.

Failure of the masonry due to compression has been observed following two mechanisms, resulting of the different stress states that are developed in the infill panel at the loaded corners and along the diagonal. The first mechanism of compressive failure can occur in the regions close to the loaded corners, where a biaxial compression-

compression stress state develops due to the lateral loading. The biaxial stress regimen improves the strength of the masonry; however the values of the stress are higher in these zones.

Flexural cracking occurs in those cases where effects are predominating and the columns of the frame are very weak, flexural

cracks can open in the tensile side of the panel due to the low tensile strength of the masonry.

3.4. Numerical Models for masonry panels

The concept of equivalent tie was introduced by Polyakov [25] after carrying out some experimental research related with in-filled frames behaviour due to horizontal loads. Polyakov [25] concluded that the wall-frame structural set has a monolithic behaviour for lower horizontal loads however as the loads are increased the lateral deformation rises too and the wall-frame behaviour becomes more complex, with detachment between the frame and the masonry panel.

In that condition, the frame suffers bending deformations and the masonry panel suffers shear deformation, remaining only the contact in the compressed corners. Then the masonry panels start to function as ties under compression only. Obviously, this type of behaviour can significantly change if there is any kind of link between the frame and the panel.

In fact it is possible to simulate the contribution of the masonry infill panel over the global structural response using diagonal ties as shown in Figure 15. These ties should have the mechanical and geometric characteristics that reproduce the behaviour of the wall and also the wall-frame structural set.

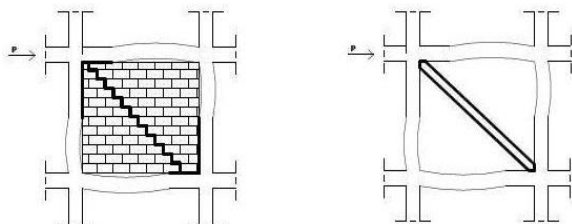


Fig. 15. Equivalent diagonal tie

The mechanical and geometric characteristics of these ties are a major issue (Stafford Smith and Carter [26]) because during the experimental results was concluded that stiffness and the diagonal resistance of the walls do not depend on their dimension and physical characteristics but on the contact length between the wall and the frame. Other authors proposed some empirical and conservative formulas with the purpose to determine the equivalent width w of the ties. Riddington and Stafford Smith [27] as well as Paulay and Priestley [28] proposed that $w=0,10 d$ and $w=0,25 d$ (where d is the diagonal length of the tie).

However, unloading and reloading is a complex phenomenon that is very difficult to be modelled accurately. Generally, the approach adopted by Crisafulli [29] is based on an analytical model that uses a curve, which passes through two predefined points (Figure 16), where the slope of the curve is known. A nonlinear continuous expression is proposed to represent the unloading-reloading curves, the main advantage of which is that the slope of the curve can be imposed at both ends.

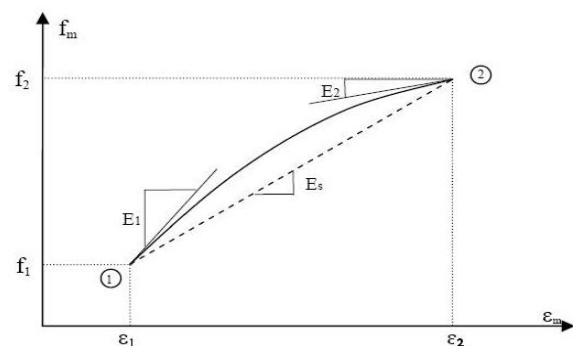


Fig. 16. Proposed curve for unloading and reloading

Experimental results indicate that the unloading curves exhibit a simple curvature and have shapes dependent on the level of unloading strain. The unloading curve (rule

2), as it is shown in Figure 17, starts from the envelope curve (ϵ_{un} , f_{un} – rule 1) and finishes with a residual or plastic deformation ϵ_{pl} , which seems to be the most important parameter in determining the unloading curve. For the prediction of the value of ϵ_{pl} , empirical expressions have been proposed but with limited validity. Crisafulli [29] expanded a general approach used earlier, introducing an empirical constant in the calculation of ϵ_{pl} .

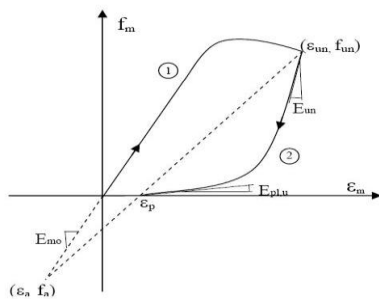


Fig. 17. Stress-strain curves for unloading branch

Figure 18 shows the reloading and unloading paths and the parameters that define such curves. The unloading curve starts when the compressive strain ϵ_m reaches the plastic strain ϵ_{pl} . After that point the compression stress increases following a path different from the one corresponding to unloading. The shape of the reloading curve is complex, showing double curvature with mild concavity in the low stress region and a sharp reversal in curvature near the envelope. The reloading curve consists of two curves. The first one (rule 4) goes from the point reloading (ϵ_{pl} , 0) to an intermediate point (ϵ_{ch} , f_{ch}). Then the second curve (rule 5) continues until the envelope curve is reached. The modulus used as final for rule 4 is used as initial for rule 5, assuring continuity. The resultant curve and its derivative are continuous,

representing thus successfully the changes of curvature observed in tests of masonry.

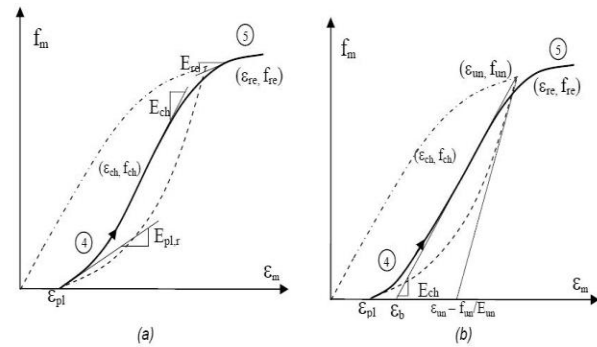


Fig. 18. (a) Reloading curve and associated parameters; (b) Definition of change point for unloading curve

The previously described rules define the loops that start from and return to the envelope curve with only one reversal after complete unloading. But reversals can happen at any place during the loading history. Also, the model proposed by Crisafulli [29] includes the effect of the inner loops. Because of the complexity of the behaviour and of lack of data, Crisafulli [29] conducted tests on standard concrete cylinders with different combinations of complete and inner loops. The conclusions drawn were: (i) the successive inner loops increase the reloading strain; (ii) the inner loops do not affect the plastic deformation; (iii) the inner loops remain inside the cycle defined for the complete unloading and reloading curves.

The former can exhibit change in direction of its concavity depending on the starting point of the loading curve, while the latter show no inflection point. A typical cyclic response with small cycle hysteresis is represented in Figure 19.

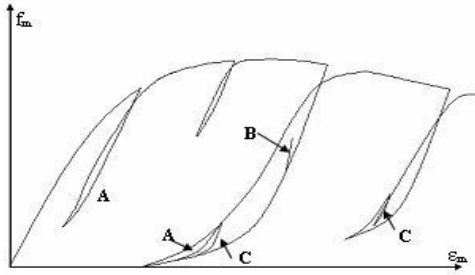


Fig. 19. Typical cyclic response with small cycle hysteresis

The adopted model is capable of representing the shear behaviour when bond failure happens along the mortar joints. It is assumed that the behaviour of the latter is linear elastic while the shear strength is not reached. Unloading and reloading are also in the elastic range. Thus, the shear stress τ is equal to the shear deformation γ times the shear modulus G_m .

The model consists of two simple rules and includes the axial load in the masonry as a variable in the shear strength. The shear strength is evaluated following a bond-friction mechanism, consisting of a frictional component and the bond strength τ_0 (elastic response – rule 1). The former depends on the coefficient of friction μ and on the compressive stress f_n perpendicular to the mortar joints.

$$\left. \begin{aligned} \tau_m &= \tau_0 + \mu |f_n| \leq \tau'_{\max} & \text{if } f_n < 0 \\ \tau_m &= \tau_0 & \text{if } f_n \geq 0 \end{aligned} \right\} \quad (12)$$

Figure 20 shows the cyclic analytical shear response of mortar joints, where τ'_{\max} represents an upper limit for the shear strength according to analytical and experimental data; somehow, for medium to high values of the compressive strength f_n , the previous equation (12) is not valid. So,

the values of μ and τ_0 should be such as to reflect the real strength of the masonry. When the shear strength is reached, the bond between mortar and brick is destroyed and cracks appear in the affected region. In this phase, one part of the infill panel slides (with respect to the other part) and only the frictional mechanism remains (sliding – rule 2).

Consequently the shear strength is given by equation (13), where μ_r is the residual coefficient of friction.

$$\left. \begin{aligned} \tau_m &= \mu_r |f_n| \leq \tau'_{\max} & \text{if } f_n < 0 \\ \tau_m &= \tau_0 & \text{if } f_n \geq 0 \end{aligned} \right\} \quad (13)$$

It is assumed that the unloading and reloading, after the bond failure, follows a linear relationship. This process can be represented by rule 1, using equation (12).

The reloading line increases the shear stress until the shear strength is reached and sliding starts again (Figure 20).

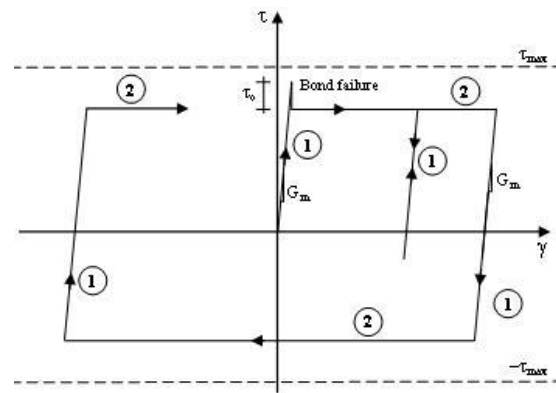


Fig. 20. Analytical response for cyclic shear response of mortar joints

Finally, it is possible to simplify the masonry infill panel behaviour as proposed by Fardis and Panagiotakos [30] and is shown in Figure 21.

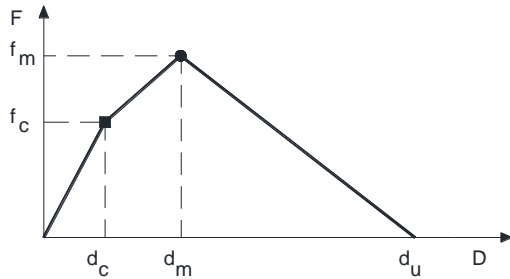


Fig. 21. Simplified masonry infill model

In this figure, the first point corresponds to the material yielding (f_c , d_c). The next point is associated to the maximum force installed in the equivalent tie (f_m , d_m). In this segment it is quite visible the occurrence of progressive stiffness degradation because the slope is smaller when comparing with the first one. That is due to the cracking

process that takes place in the panel, leading to a structural stiffness reduction (Cesar, Oliveira and Barros [20]). Finally, the last point is related with panel collapse at ultimate displacement D_u .

3.5 Examples of R/C infilled frames pushover analysis

In this study several configurations of a regular R/C frame will be analysed. It is intended to simulate several asymmetries in order to compute the structural performance of each configuration and compare the resistant capacity evolution during the pushover procedure. The chosen structural configurations are shown in Figure 22.

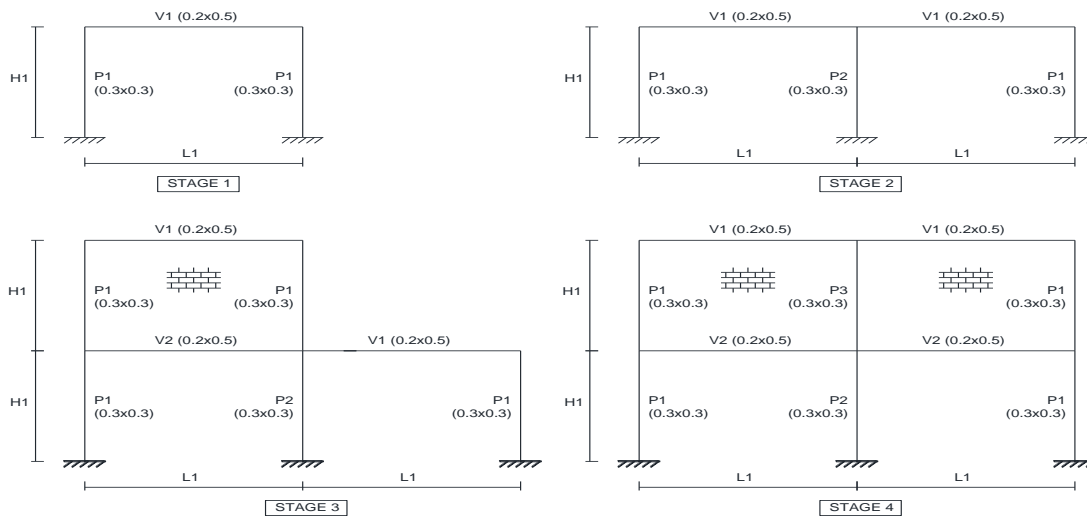


Fig. 22. Pushover analysis evaluative steps, along four configurations stages

The R/C members are made of C30/37 concrete and S500 steel grade and were designed according to Eurocode 2 (EC2)

[31]. According with this design procedure, the columns and beams must have the following cross section: upper beams (0.2x0.5 m²), lower beams (0.3x0.6 m²) and columns (0.3x0.3 m²). The reinforcement distribution of each cross section is shown in Figure 23.

In this study will be adopted two load pattern distributions (uniform and modal distributions) as presented in EC8 [2]. To obtain the moment-rotation constitutive law of each cross section, i.e. the hinge behaviour, FAGUS [32] software was used.

To develop the parametric study a set of spans (5.0, 6.0 and 7.0 m) and inter-story heights (3.0, 3.5 and 4.0 m) were used. The nonlinear static Pushover analyses used and

compared three software packages: SAP 2000 [33], MIDAS/CIVIL [18] and SeismoStruck [34].

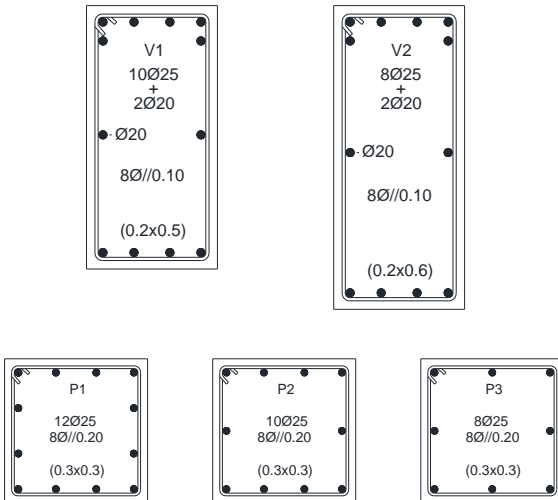


Fig. 23. R/C section for beams and columns

The pushover analyses were made based on concentrated hinges located near the end of each structural element. Usually, the distance between the concentrated hinge and the ex-tremity of the element is half the length of the hinge.

SeismoStruck software has some appropriate features to model RC frame pushover with distributed nonlinearity. It uses a three-dimensional fiber model based on finite elements, and all the analyses are treated as potentially nonlinear considering material and geometric non-linearity. The distribution

of inelasticity along the length of the elements is modelled through a cubic approximation that allows a precise estimative of the damages. The tension-extension state of the elemental sections is obtained integrating the individual nonlinear and uniaxial response of each fiber in which the section of the member element was divided. In order to integrate the equations of the cubic interpolation functions that govern the nonlinear response, two Gauss points per element are used.

The masonry panel used in this study has a young modulus of 6.0 GPa and a self-weight of 2.2 kN/m². The masonry was modelled as an equivalent tie in SAP 2000 and MIDAS, and two different masonry behaviour models were used with SeismoStruck: “Masonry infill strut curve” (Inf_strut) and “Masonry infill shear curve” (Inf_Shear). Both models were developed and initially programmed by Crisafulli [29], and were introduced later in the program by Blandon [30].

The parameters involved in the equivalent tie model used to simulate the infill panel are shown in Table 4. Due to difficulties developing a general model that could cover all the potential modes of failure, only some of them were considered: cracking associated to shear and compressive failure of the equivalent ties.

Table 4. Simplified masonry model

Equivalent tie behavioral model					
f_c (kN)	f_c (m)	f_m (kN)	d_m (m)	f_u (kN)	d_u (m)
110	0,001	135	0,075	0	0,3

Based on the mentioned parameters, the following results were obtained: (i) global capacity curves under several load pattern distributions; (ii) variation of the maximum basal shear in the structure according to the

parametric study; and finally: (iii) the maximum relative displacement between floors (floor drifts) for the defined load patterns.

For stage 1 and 2 (a single storey) only uniform distribution will be addressed because all the load patterns are essentially the same. Furthermore, the influence of masonry panels will only be studied for stage 3 and 4 (since usually the first floor of office buildings is almost entirely glazed). Although the initial parametric study involved several beam spans and inter-storey heights, it was observed that the worst scenario is obtained with the highest value of these parameters (beam spans of 7.0m meters and inter-storey height of 4.0 m). In this case, only the results based on these values will be presented.

1st Configuration (Stage One)

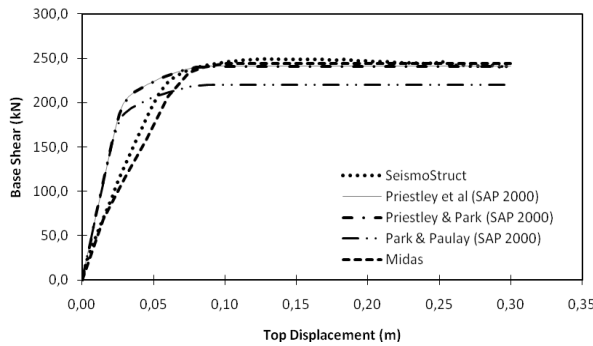


Fig. 24. Capacity curves – Stage one

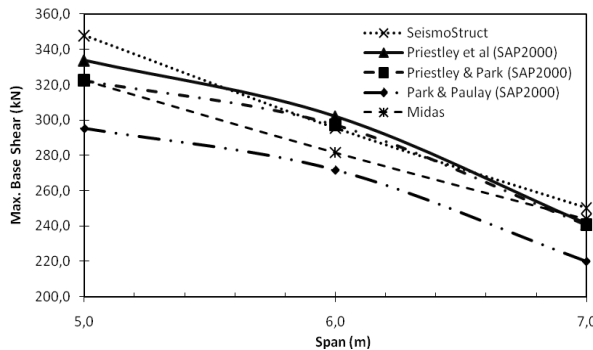


Fig. 25. Maximum base shear variation

2nd Configuration (Stage Two)

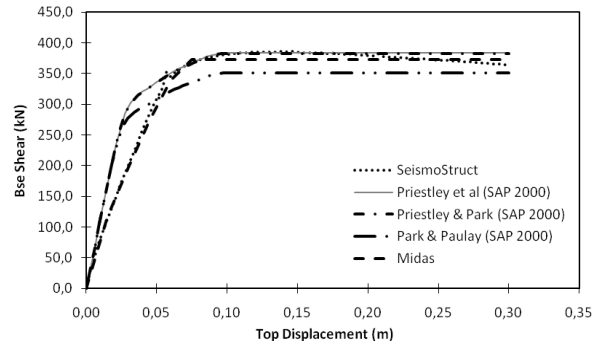


Fig. 26. Capacity curves

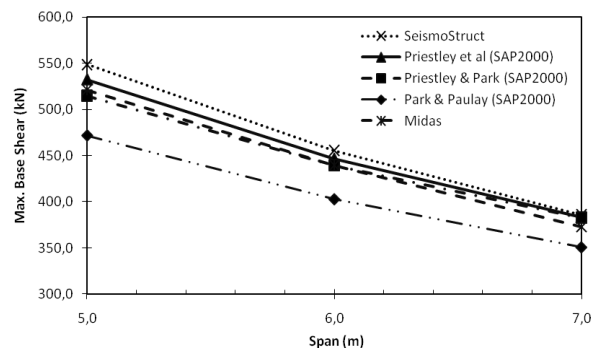


Fig. 27. Maximum base shear variation

3rd Configuration (Stage Three)

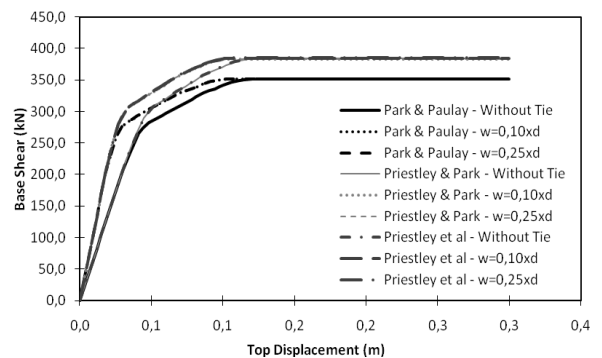


Fig. 28. Capacity curves with uniform load pattern using SAP 2000

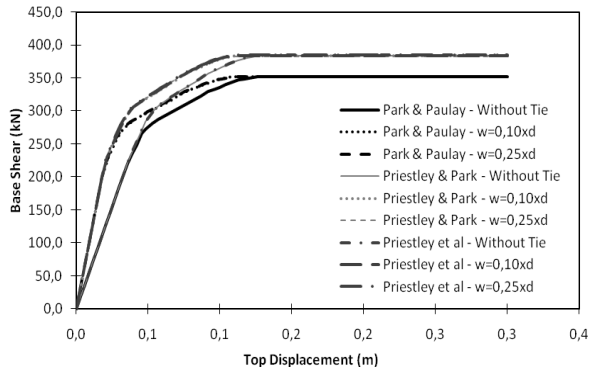


Fig. 29. Capacity curves with modal load pattern using SAP 2000

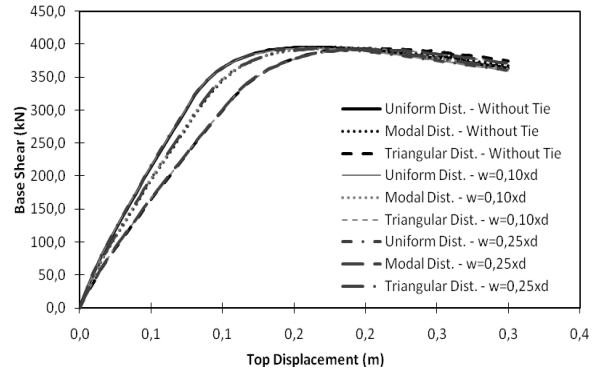


Fig. 32. Capacity curves for all types of load pattern distributions (SeismoStruck)

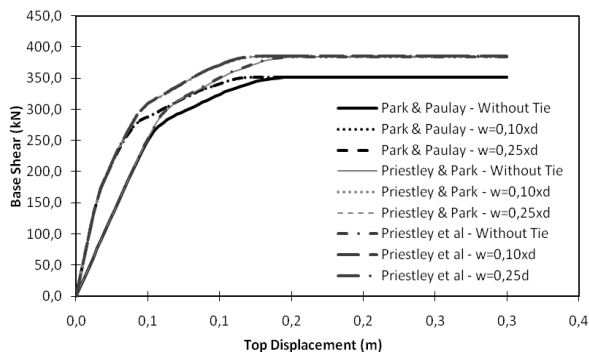


Fig. 30. Capacity curves with triangular load pattern using SAP 2000

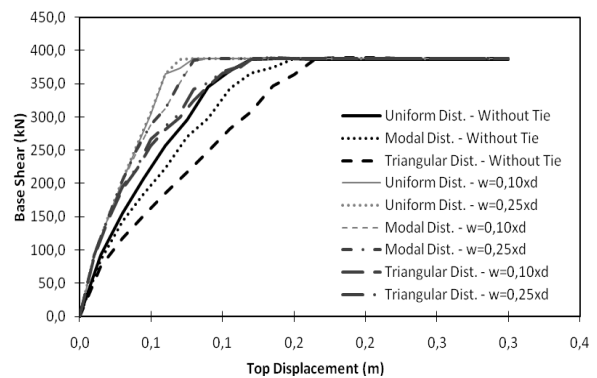


Fig. 33. Capacity curves for all types of load pattern distributions (MIDAS/CIVIL)

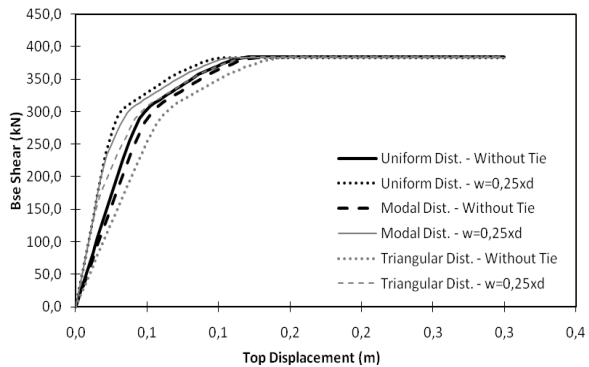


Fig. 31. Capacity curves (Priestley et al [24]) for all types of load pattern distributions (SAP 2000)

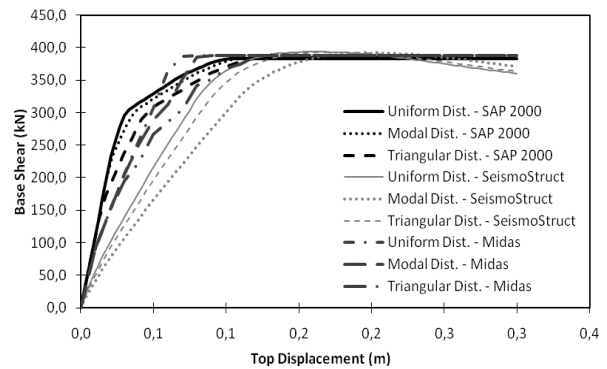


Fig. 34. Comparison of the capacity curves (3 software) for all types of load pattern distributions

The maximum drifts verified in those analyses are presented in the following tables:

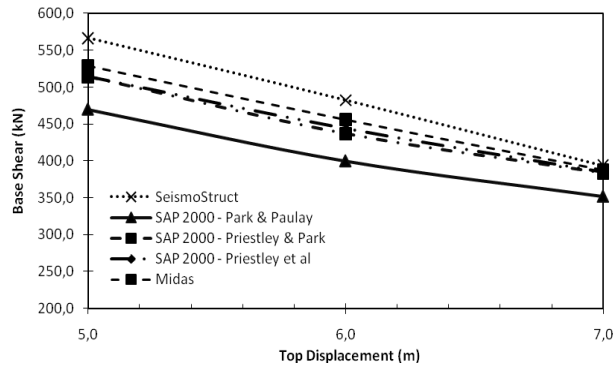


Fig. 35. Maximum base shear (uniform dist.) with $w=0.25xd$

Table 5. Drifts using the proposal of Priestley et al [24] for all load pattern distributions (SAP 2000)

Drifts - Stage 3 - SAP 2000			
Uniform distribution			
Storey's	Priestley et al		
	w/ tie	w=0,10xd	w=0,25xd
R/C – 1° Floor	0,2789	0,2922	0,2950
1° Floor – 2° Floor	0,0211	0,0050	0,0050
Modal distribution			
Storey's	Priestley et al		
	w/ tie	w=0,10xd	w=0,25xd
R/C – 1° Floor	0,2724	0,2870	0,2887
1° Floor – 2° Floor	0,0276	0,0125	0,0113
Triangular distribution			
Storey's	Priestley et al		
	w/ tie	w=0,10xd	w=0,25xd
R/C – 1° Floor	0,2550	0,2775	0,2775
1° Floor – 2° Floor	0,0450	0,0225	0,0225

Table 6. Drifts obtained with SeismoStruck [34] for all load pattern distributions

Drifts - Stage 3- SeismoStruck			
Uniform distribution			
Storey's	w/ tie	w=0,10xd	w=0,25xd
	R/C – 1° Floor	0,12578	0,12622
1° Floor – 2° Floor	0,03686	0,03641	0,03778
Modal distribution			
Storey's	w/ tie	w=0,10xd	w=0,25xd
	R/C – 1° Floor	0,12914	0,12730
1° Floor – 2° Floor	0,04871	0,04753	0,04725
Triangular distribution			
Storey's	w/ tie	w=0,10xd	w=0,25xd
	R/C – 1° Floor	0,13646	0,13442
1° Floor – 2° Floor	0,0748	0,07383	0,07336

Table 7. Drifts obtained with MIDAS/CIVIL [18] for all load pattern distributions

<i>Stage 3</i>			
Uniform distribution			
Storey's	w/ tie	w=0,10xd	w=0,25xd
R/C – 1° Floor	0,248	0,292	0,293
1° Floor – 2° Floor	0,052	0,008	0,007
Modal distribution			
Storey's	w/ tie	w=0,10xd	w=0,25xd
R/C – 1° Floor	0,241	0,280	0,282
1° Floor – 2° Floor	0,059	0,020	0,018
Triangular distribution			
Storey's	w/ tie	w=0,10xd	w=0,25xd
R/C – 1° Floor	0,191	0,195	0,259
1° Floor – 2° Floor	0,079	0,045	0,041

4th Configuration (Stage Four)

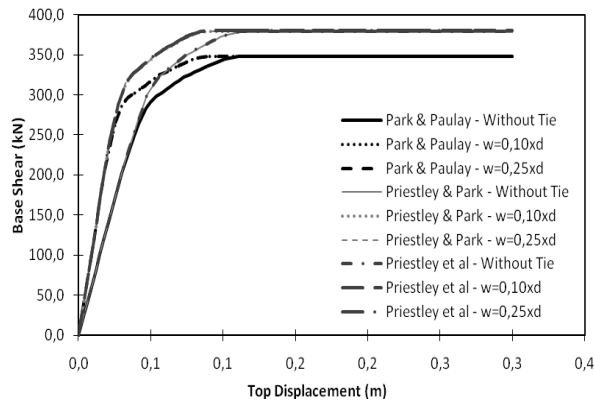


Fig. 36. Capacity curves with uniform load pattern using SAP 2000

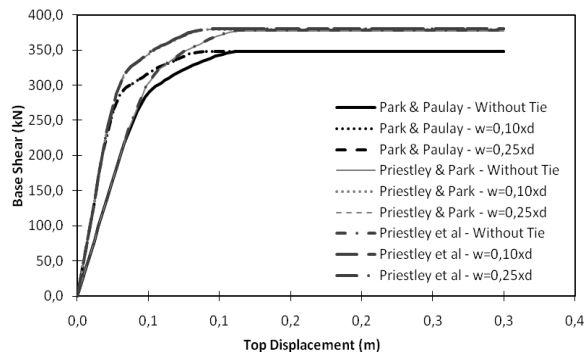


Fig. 37. Capacity curves with modal load pattern using SAP 2000

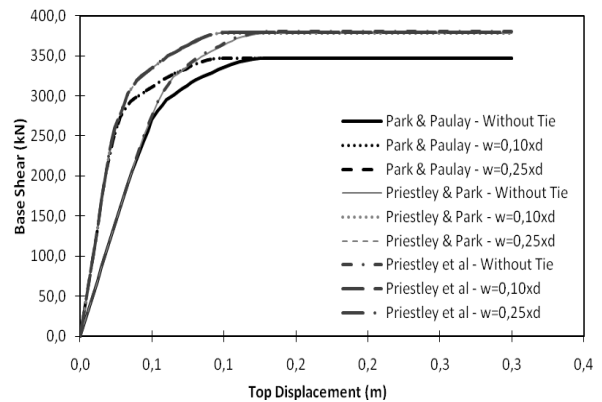


Fig. 38. Capacity curves with triangular load pattern using SAP 2000

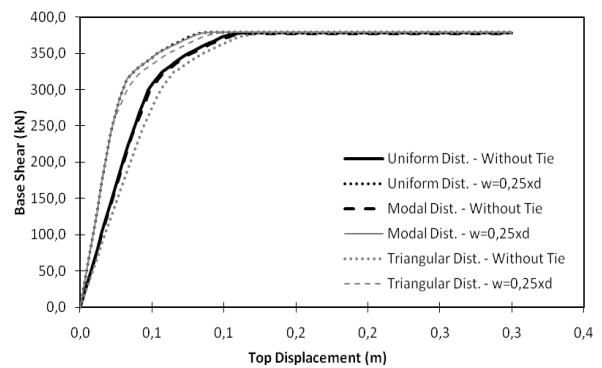


Fig. 39. Capacity curves (Priestley et al [24]) for all types of load pattern distributions (SAP 2000)

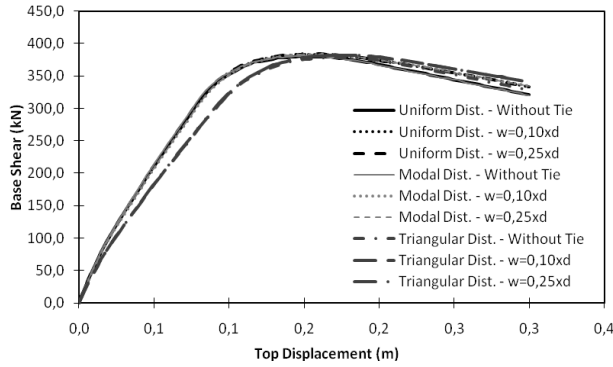


Fig. 40. Capacity curves for all types of load pattern distributions (SAP 2000)

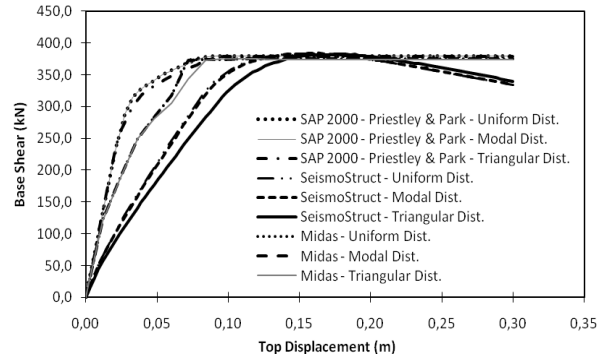


Fig. 42. Comparison of the capacity curves (3 software) for all types of load pattern distributions

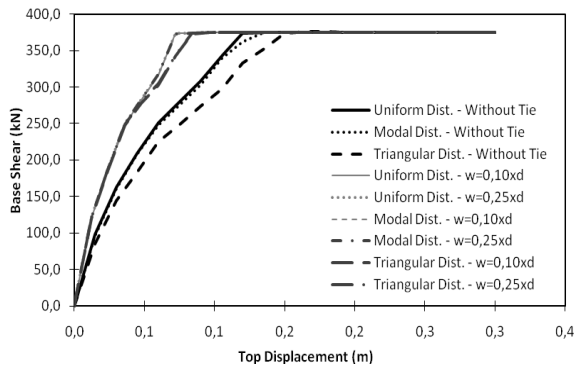


Fig. 41. Capacity curves for all types of load pattern distributions (MIDAS/CIVIL)

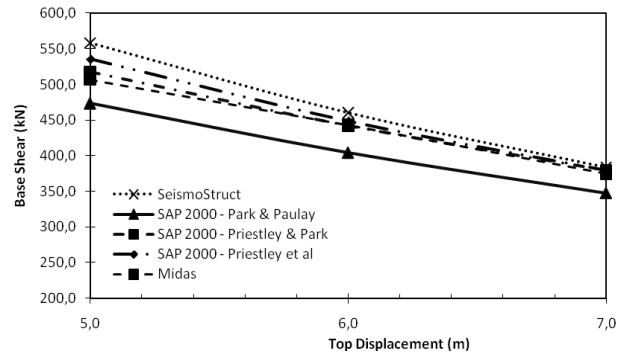


Fig. 43. Maximum base shear (uniform dist.) with w=0.25xd

Comparison of capacity curves obtained from the three software used:

Table 8. Drifts corresponding to proposal of Priestley et al [24] for all load patterns, using SAP 2000

Stage 4			
Uniform distribution			
Storey's	Priestley et al		
	w/ tie	w=0,10xd	w=0,25xd
R/C – 1° Floor	0,2782	0,2990	0,2989
1° Floor – 2° Floor	0,0218	0,0010	0,0011
Modal distribution			
Storey's	Priestley et al		
	w/ tie	w=0,10xd	w=0,25xd
R/C – 1° Floor	0,2771	0,2961	0,2979
1° Floor – 2° Floor	0,0229	0,0027	0,0021
Triangular distribution			
Storey's	Priestley et al		
	w/ tie	w=0,10xd	w=0,25xd
R/C – 1° Floor	0,2675	0,2903	0,2903
1° Floor – 2° Floor	0,0325	0,0097	0,0097

Table 9. Drifts obtained with SeismoStruck [34] considering all load pattern distributions

Stage 4			
Uniform distribution			
Storey's	w/ tie	w=0,10xd	w=0,25xd
R/C – 1° Floor	0,12442	0,12509	0,12545
1° Floor – 2° Floor	0,03817	0,03749	0,03712
Modal distribution			
Storey's	w/ tie	w=0,10xd	w=0,25xd
R/C – 1° Floor	0,12532	0,12613	0,12649
1° Floor – 2° Floor	0,04031	0,03948	0,03912
Triangular distribution			
Storey's	w/ tie	w=0,10xd	w=0,25xd
R/C – 1° Floor	0,1284	0,12345	0,12385
1° Floor – 2° Floor	0,05538	0,05432	0,05391

Table 10. Drifts obtained with MIDAS/CIVIL [18] considering all load pattern distributions

Stage 4			
Uniform distribution			
Storey's	w/ tie	w=0,10xd	w=0,25xd
R/C – 1° Floor	0,260	0,296	0,297
1° Floor – 2° Floor	0,040	0,004	0,003
Modal distribution			
Storey's	w/ tie	w=0,10xd	w=0,25xd
R/C – 1° Floor	0,258	0,295	0,295
1° Floor – 2° Floor	0,042	0,005	0,005
Triangular distribution			
Storey's	w/ tie	w=0,10xd	w=0,25xd
R/C – 1° Floor	0,237	0,285	0,287
1° Floor – 2° Floor	0,063	0,015	0,013

The capacity curves obtained by the MIDAS/CIVIL [18] show that the ascending branch follows closely the one obtained with the SeismoStruck [34]. Moreover the final branch of the curves, which is the maximum basal shear of the structure, is very near to the one obtained with SeismoStruck and even with SAP 2000 by the joint proposals of Park et al [9] and Priest-ley et al [10]. It can also be concluded that the yielding of the RC frame sections occurs earlier for the joint proposals made in the SAP 2000 in comparison to MIDAS/CIVIL [18] and SeismoStruck [34].

Moreover, the curves obtained in stage 3 and 4 show that when equivalent ties (with widths of 10% and 25% of the diagonal length of the panel) are used there was not a major difference in the capacity curves obtained. Although, considering the assumptions of absence of tie and a tie with a thickness equal to 25%, there is a certain difference in the curves (with the ascending branch slightly different). With the inclusion of the ties in the model, there is greater stiffness in the structure so that the top displacements are smaller.

Thus a constant reduction of top displacement for the same basal shear value

is observed. However, all the curves converge to the same maximum basal shear value.

Adopting the triangular load distribution, a greater discrepancy in the curves under the various proposals is surely seen, which is very evident in the curves obtained by MIDAS/CIVIL. Moreover, the clearly seen bundle of curves represented is due to a greater parametric variability. It was also observed that the curves obtained with the uniform and modal distribution are close enough comparing to the triangular one.

Finally, the maximum inter-storey displacements were calculated, showing that between the ground floor and 1st floor the drifts are more significant in SAP 2000 [33] and MIDAS/CIVIL [18], while the relative displacements between 1st and 2nd floors are higher in SeismoStruck [34]. This difference observed, more specifically between the last two floors, can be justified based on the behavioural models embedded in SeismoStruck [34] in which two modes of failure are included: compressive failure of the equivalent tie and shear failure. In other words, the redistribution of stress according with the possible modes of failure included in this program and their interaction leads to higher collapse resistance values compared to SAP 2000 [33] and MIDAS/CIVIL [18], therefore, also the drifts are higher when SeismoStruck [34] is used.

Disregarding the influence of masonry panels on the 2nd floor, it appears that the relative displacements between the last floors are higher because there is not enough stiffness in the structure when compared with the equivalent ties consideration. Moreover, the modal and uniform distributions are indeed the ones that

become closest, which is evident in the results obtained by SeismoStruck [34]. The structure with 1 or 2 levels shows different behaviour for modal and triangular distributions while in the multi-storey structures a similar behaviour is obtained. In this case, the modal and triangular distributions become very close because the fundamental mode controls the response of the structure.

4. CONCLUSIONS

The main objective of this work consisted on the presentation of a simplified methodology (pushover analyses) that allows obtaining the response of a structure under seismic actions considering its non-linear behaviour. To reach the objective several steel and RC frames were studied. The steel structures (3, 6 and 10 floors) were analyzed under seismic loading (considered applied in two alternative loading patterns) with three variations of their resistant structural system (with and without bracing). To complete the study several RC frames with and without masonry infill panels were analysed based on some numerical models proposed in commercial software.

In these analyses it was verified that this pushover methodology allows evaluating the performance of structures through control of their displacements (at local and global levels), still giving additional information about the ductility and the resistant capacity. The introduction of bracing members in the steel structures influences significantly the obtained results, altering the resistant capacity and the associated collapse mode. This contribution allows improving the knowledge about the seismic response of the analyzed structures, above all for the

redistribution of the damaged zones during the occurrence of a high intensity earthquake.

The response of the structures is sensitive to the loading pattern justifying the adoption of an envelope of the resistant capacity associated to the possible loading patterns. In the studied structural cases, it was verified that the largest resistant capacity was obtained with a uniform distribution of the lateral loads. Pushover analysis started to be implemented in the seismic regulations because it is an advantageous methodology for the evaluation of the seismic performance of structures, therefore justifying this present study and the need for continuing this research to better evaluate and characterize the applications of these analyses.

ACKNOWLEDGEMENTS

Special thanks are also due to Prof. Rui Pinho at Rose School of the University of Pavia, for providing the version used of SeismoStruck and for the rich exchange of information between our institutions.

REFERENCES

- [1] Fajfar, P., Fischinger, M. "N2 – A Method for Non-Linear Seismic Analysis of Regular Buildings". Proceedings of the 9th World Conference in Earthquake Engineering, 1988, Vol.5, 111-116, Tokyo-Kyoto, Japan.
- [2] EC 8, Eurocode 8: Design of structures for earthquake resistance; Part 1: General Rules, Seismic Actions and Rules for Buildings; CEN, Brussels, 2003.
- [3] Cesar, M.B., Barros, R.C., "Estudo Preliminar sobre o Desempenho Sísmico de Pórticos Metálicos Contraventados a partir de Análises Estáticas Não-Lineares (Pushover)"; Proceedings of 'Métodos Numéricos e Computacionais em Engenharia CMNE 2007 e XXVIII CILAMCE', Congresso Ibero Latino-Americano sobre Métodos Computacionais em Engenharia, FEUP, Porto, 13-15 Junho 2007; CMNE/CILAMCE 2007, Paper 1184 – pp. 1-18; Edts: A. Rodriguez-Ferran, Javier Olivier, Paulo R.M. Lyra, José L.D. Alves; APMTAC / SEMNI, 2007.
- [4] Cesar, M.B., Barros, R.C., "Seismic Performance of Metallic Braced Frames by Pushover Analyses", Computational Methods in Structural Dynamics and Earthquake Engineering (COMPDYN 2009), M. Papadrakakis, N.D. Lagaros, M. Fragiadakis (eds.), Rhodes, Greece, 22–24 June 2009.
- [5] Pereira, V.G., Barros, R.C. and Cesar, M.B., "A Parametric Study of a R/C Frame Based on Pushover Analysis", 3rd International Conference on Integrity, Reliability & Failure (IRF 2009), J.F. Silva Gomes and S.A. Meguid (eds.), Porto, Portugal, 20-24 July 2009.
- [6] Pereira, V.G., Barros, R.C. and Cesar, M.B., "Pushover Analyses of a R/C Frame by distinct Software", 12th International Conference on the Enhancement and Promotion of Computational Methods in Engineering and Science (EPMESC XII), Hong-Kong and Macao, 30 Nov–3 Dec 2009.
- [7] Elghazouli, A.Y. (editor), "Seismic Design of Buildings to Eurocode 8", Spon Press, Abingdon, Oxon, UK, 2009.
- [8] FEMA - Federal Emergency Management Agency, "NEHRP guidelines for the seismic rehabilitation of buildings", FEMA-273; "NEHRP commentary on the guidelines for the seismic rehabilitation of buildings", FEMA-274; Washington, D.C., 1997.
- [9] R.F. Almeida, R.C. Barros, "A new multimode load pattern for pushover analysis: the effect of higher modes of vibration", Earthquake Resistant Engineering Structures IV, Eds.: G. Latini

- and C.A. Brebbia, WIT Press, (2003), U.K., pp. 3-13.
- [10] R. C. Barros, R. Almeida, "Pushover analysis of asymmetric three-dimensional buildings frames", *Journal Civil Engineering & Management*, Vol. XI, Number 1, pp. 3-12, Vilnius, Lithuania, 2005.
- [11] Chopra, A.K., Goel, R.K., "A modal pushover analysis procedure to estimate seismic demands for unsymmetric-plan buildings", *Earthquake Engng Struct. Dyn.* 33: 903–927, John Wiley & Sons Ltd, 2004.
- [12] H.N. Li, G. Li, Simplified method for pushover curves of asymmetric structure with displacement dependent passive energy dissipation devices, *Advances in Structural Engineering*, Vol. 10, Issue 5, (2007), 537-649.
- [13] G. Li, H.N. Li, Direct displacement-based design for buildings with passive energy dissipation devices, *Gongcheng Lixue/Engineering Mechanics*, Vol. 25, Issue 3, (2008), 49-57.
- [14] ATC, Seismic evaluation and retrofit of concrete buildings, Report ATC-40, Applied Technology Council, Redwood City CA (1996).
- [15] FEMA-356, Prestandard and commentary for the seismic rehabilitation of buildings, Report FEMA 356, Federal Emergency Management Agency, Washington, (2000).
- [16] P. Fajfar, A nonlinear analysis method for performance-based seismic design, *Earthquake Spectra*, Vol. 16, EERI, (2000), pp. 573-592.
- [17] R. Bento, S. Falcão, F. Rodrigues, Avaliação sísmica de estruturas de edifícios com base em análises estáticas não lineares, *SISMICA 2004 – 6º Congresso Nacional de Sismologia e Engenharia Sísmica*, Guimarães, Portugal, 2004.
- [18] MIDASIT, "MIDAS/Civil – General purpose analysis and optimal design system for civil structures", MIDAS Information Technology Co, Ltd., Korea, 2005.
- [19] M.S. Williams, F. Albermani, Evaluation of displacement-based analysis and design methods for steel frames with passive energy dissipators, *Civil Engineering Research Bulletin No. 24*, University of Queensland, Australia, 2003.
- [20] Braz-Cesar, M., Oliveira, D.V. and R. Carneiro-Barros, "Numerical Validation of the Experimental Cyclic Response of RC Frames", Chapter 12 in the book *Trends in Computational Structures Technology*, Edited by: B.H.V. Topping, Saxe-Coburg Publications, ISBN 978-1-874672-39-5, pp. 267-291, Stirlingshire, Scotland, 2008.
- [21] H. Krawinkler, G.D.P.K. Seneviratna, Pros and cons of a pushover analysis of seismic performance evaluation, *Engineering Structures*, Vol. 20, (1998), pp. 452-464.
- [22] Park, R. and T. Paulay, *Reinforced Concrete Structures*. John Wiley & Sons Inc., New York, 1975.
- [23] Park, R., Priestley, M.J.N., and W.D. Gill; "Ductility of square-confined concrete columns", *Journal of the Structural Division, ASCE*, Vol. 108, No. ST 4, pp. 929-950, 1982.
- [24] Priestley, M.J.N., Seible, F. and G.M.S. Calvi, *Seismic design and retrofit of bridges*. John Wiley & Sons Inc., New York, 1996.
- [25] Polyakov, S. V., *Masonry in framed building: an investigation into the strength and stiffness of masonry infilling*, Moscow, 1957.
- [26] Stafford Smith, B. and C. Carter, "A method of analysis for infilled frames", *Proceedings of the Institution of Civil Engineers*, Vol. 44, 1969.
- [27] Riddington, J. R. and B. Stafford Smith, "Analysis of infilled frames subject to racking with design recommendations", *The Structural Engineer*, Vol. 55, N° 6, 1977.
- [28] Paulay, T. and M. Priestley, *Seismic Design of Reinforced Concrete and Masonry Buildings*, John Wiley & Sons, 1992.

- [29] Crisafulli F.J., Seismic Behaviour of Reinforced Concrete Structures with Masonry Infills, PhD Thesis, University of Canterbury, New Zealand, 1997.
- [30] Fardis, M.N. and T.B. Panagiotakos, "Seismic design and response of bare and masonry-infilled reinforced concrete buildings – Part II: Infilled structures", *Journal of Earth-quake Engineering*, Vol. I, No 3, 475-503, 1997.
- [31] Eurocódigo 2: Projecto de estruturas de betão; Parte 1-1: Regras gerais e regras para edifícios. Comité Europeu de Normalização, Brussels, 2004.
- [32] Fagus, Fagus-5: Version 1.22.0 Build 275, Cubus AG, Zürich, 2000-2006.
- [33] Computers & Structures Inc.; "SAP 2000 v10.0.1 – Structural Analysis Program". Berkeley, California, U.S.A., 2005.
- [34] SeismoSoft SeismoStruck, "A Computer Program for Static and Dynamic Nonlinear Analysis of Framed Structures". Available online at: <http://www.seismosoft.com>; 2006.
- [35] Blandon, C.A., "Implementation of an Infill Masonry Model for Seismic Assessment of Existing Buildings", Individual Study, European School for Advanced Studies in Reduction of Seismic Risk (ROSE School), Pavia, Italy, 2005.